THE JOURNAL OF BIOLOGICAL CHEMISTRY VOL. 291, NO. 30, pp. 15853–15866, July 22, 2016

CHD4 Is a Peripheral Component of the Nucleosome Remodeling and Deacetylase Complex*

Received for publication, November 26, 2015, and in revised form, May 16, 2016 Published, JBC Papers in Press, May 27, 2016, DOI 10.1074/jbc.M115.707018

Jason K. K. Low[‡1], Sarah R. Webb[‡1,2], Ana P. G. Silva[‡3], Hinnerk Saathoff[‡3], Daniel P. Ryan[§], Mario Torrado[‡], Mattias Brofelth[‡], Benjamin L. Parker[‡], Nicholas E. Shepherd[‡4], and Joel P. Mackay[‡5]

From the [‡]School of Life and Environmental Sciences, University of Sydney, Sydney, New South Wales 2006, Australia and the [§]Department of Genome Sciences, John Curtin School of Medical Research, Australian National University, Acton, Australian Capital Territory 2601, Australia

Chromatin remodeling enzymes act to dynamically regulate gene accessibility. In many cases, these enzymes function as large multicomponent complexes that in general comprise a central ATP-dependent Snf2 family helicase that is decorated with a variable number of regulatory subunits. The nucleosome remodeling and deacetylase (NuRD) complex, which is essential for normal development in higher organisms, is one such macromolecular machine. The NuRD complex comprises ~10 subunits, including the histone deacetylases 1 and 2 (HDAC1 and HDAC2), and is defined by the presence of a CHD family remodeling enzyme, most commonly CHD4 (chromodomain helicase DNA-binding protein 4). The existing paradigm holds that CHD4 acts as the central hub upon which the complex is built. We show here that this paradigm does not, in fact, hold and that CHD4 is a peripheral component of the NuRD complex. A complex lacking CHD4 that has HDAC activity can exist as a stable species. The addition of recombinant CHD4 to this nucleosome deacetylase complex reconstitutes a NuRD complex with nucleosome remodeling activity. These data contribute to our understanding of the architecture of the NuRD complex.

Nucleosomes effectively act as a roadblock to all aspects of genome biology. ATP-dependent chromatin remodeling enzymes solve this problem by using ATP-derived energy to alter the positions, occupancy and composition of nucleosomes. All remodelers possess a highly related ATPase motor domain from the helicase family and are classified into four subfamilies (INO80, ISWI, SWR1, and CHD) based on sequence similarity (1). Each subfamily is represented in nearly all eukaryotes, suggesting that they catalyze different remodeling events. For example, ISWI proteins reposition (or slide) nucleosomes to create regularly spaced arrays; this periodic organization is a key characteristic of DNA at the start of genes (2). SWR1 and INO80 enzymes have opposing roles in histone variant dynamics; the former incorporates these histone variants (*e.g.* H2A.Z), whereas the latter removes them. These variants set up specific chromatin structures that modulate transcription and replication, although the roles of many variants are still under debate (3). Fundamentally, these remodeling enzymes all alter the accessibility of DNA to other DNA-binding factors and thereby broadly underpin genome biology.

Remodelers frequently act in the context of large multisubunit complexes, and in general, the "mixing and matching" of complex composition can generate complexes with varying activities; the human ISWI protein Snf2h for instance has been identified in six distinct complexes (4). Likewise, the accessory subunits can also modulate remodeler activity. For example, the paralogous methyl-CpG-binding domain proteins 2 and 3 (MBD2 and MBD3) subunits of the nucleosome remodeling and deacetylase (NuRD)[6] complex are mutually exclusive (5); MBD2 recognizes 5-methylcytosine-modified DNA, whereas MBD3 instead binds to 5-hydroxymethylated DNA (6, 7). Unsurprisingly, it has been observed that MBD2 guides the NuRD complex to repressed, methylation-rich loci in the genome, whereas MBD3 has been observed to localize to active, unmethylated chromatin (8).

Although there have been considerable advances made in our understanding of the structure and function of chromatin remodeling complexes, a detailed mechanistic description of remodeling is still lacking, and no high resolution structures of remodeling complexes are available. A number of low resolution models of these remodeling complexes (23–50 Å) derived from single-particle electron microscopy and cryo-EM data have been reported (9–17); these models reveal some diversity in the overall shape of each complex, but a common feature is the integral nature of the remodeling subunit. For example, in the recent INO80 and SWR1 structures, the Ino80 and Swr1 ATPases lie at the center of the corresponding complex and are decorated with sets of regulatory subunits (14, 16).

The NuRD complex is a broadly expressed chromatin remodeling complex that is found only in complex organisms

* This work was supported by Australian Research Council Grant DE120102857 and National Health and Medical Research Council Grants APP1012161, 1063301, and 571099. The authors declare that they have no conflicts of interest with the contents of this article.

[1] These authors contributed equally to this work.
[2] Present address: Francis Crick Institute, Mill Hill Laboratory, The Ridgeway, Mill Hill, London, UK.
[3] These authors contributed equally to this work.
[4] To whom correspondence may be addressed. Present address: Institute of Molecular Bioscience, The University of Queensland, St. Lucia, QLD 4072, Australia. Tel.: 61-7-33462991; Fax: 61-7-33462101; E-mail: n.shepherd@imb.uq.edu.au.
[5] To whom correspondence may be addressed: School of Life and Environmental Sciences, Bldg. G08, University of Sydney, NSW 2006, Australia. Tel.: 61-2-93513906; Fax: 61-2-93514726; E-mail: joel.mackay@sydney.edu.au.

[6] The abbreviations used are: NuRD, nucleosome remodeling and deacetylase; HDAC, histone deacetylase; NuDe, nucleosome deacetylase; MTA, metastasis-associated protein; MEL, murine erythroleukemia; CV, column volumes; Tricine, *N*-[2-hydroxy-1,1-bis(hydroxymethyl)ethyl]glycine.

and that has important roles in gene regulation (18) and DNA repair (19). NuRD activity is essential at all stages of hematopoiesis, regulating both hematopoietic stem cell maintenance and differentiation of these cells into distinct lineages (20–22). Aberrant expression of NuRD subunits is also strongly linked to cancer (23), and the down-regulation of several NuRD components induces changes in chromatin structure that are associated with aging (24). NuRD is also emerging as a significant and perhaps controversial player in efforts to reprogram somatic cells into pluripotent stem cells (25–27).

The most frequently observed subunits of the NuRD complex are a remodeler (CHD4, CHD3, or CHD5); the histone deacetylases HDAC1 and HDAC2; the WD40 repeat proteins RBBP4 and RBBP7; the metastasis-associated proteins MTA1, MTA2, and MTA3; the poorly defined proteins GATAD2A and GATAD2B; and the methyl-DNA binding domain proteins MBD2 and MBD3. In each case, the alternative proteins are closely related (*e.g.* human HDAC1 and HDAC2 are 86% identical), and overall we know very little about the relative distributions of these orthologues in the complex and what functional changes might be imparted by changes in subunit composition.

Three structures of subcomplexes have been reported: (i) HDAC1 bound to a fragment of MTA1 (28); (ii) a dimeric coiled coil formed by ~40-residue segments of GATAD2A and MBD2 (29); and (iii) RBBP4 bound to a short peptide from MTA1 (30). Stoichiometry data derived from label-free mass spectrometry measurements also provide hints about the number of copies of each subunit that come together in the complex (31, 32), although the mass spectrometric data do not seem entirely consistent with the structural data. However, in contrast to the remodeling complexes described above, nothing is known about the overall architecture of the NuRD complex (Note added in proof).

NuRD is invariably depicted in the literature as a multisubunit complex with the remodeling subunit CHD4 as the central hub protein (18, 33–35). This interpretation is consistent with the structures of other chromatin remodeling complexes such as SWR1 and INO80. Here, we demonstrate that CHD4 is in fact a peripheral component of the NuRD complex and that an otherwise fully intact complex with histone deacetylase activity can exist, at least *in vitro*, in the absence of CHD4. These data suggest that the NuRD complex might act via a mechanism that is distinct from other remodeling complexes and perhaps provides a mechanism by which CHD4 can disengage easily from NuRD to carry out functions independent of the remainder of the complex.

Results

NuRD Forms a Stable Complex in the Absence of CHD4—In previous work, Hong *et al.* (36) demonstrated that the NuRD complex could be purified from murine erythroleukemia (MEL) cell extracts by a single-step affinity chromatography method using an N-terminal GST fusion of the first 45 residues of the transcriptional co-regulator FOG1(1–45) (Friend of GATA1). It was further shown that this FOG1-NuRD interaction appears to be mostly mediated by the MTA and RBBP family proteins (36, 37). Recently, we showed that good purification could be achieved using a synthetic version of FOG1(1–15) with a C-terminal fusion of the StreptagII peptide affinity tag and a fluorescein moiety (for ease of detection purposes) (38). Importantly, using these FOG1 affinity chromatography methods, relatively clean NuRD preparations can be achieved despite the fact that several components of the NuRD complex (*e.g.* HDACs and RBBPs) are also key components in other complexes, such as the SIN3 deacetylase complex.

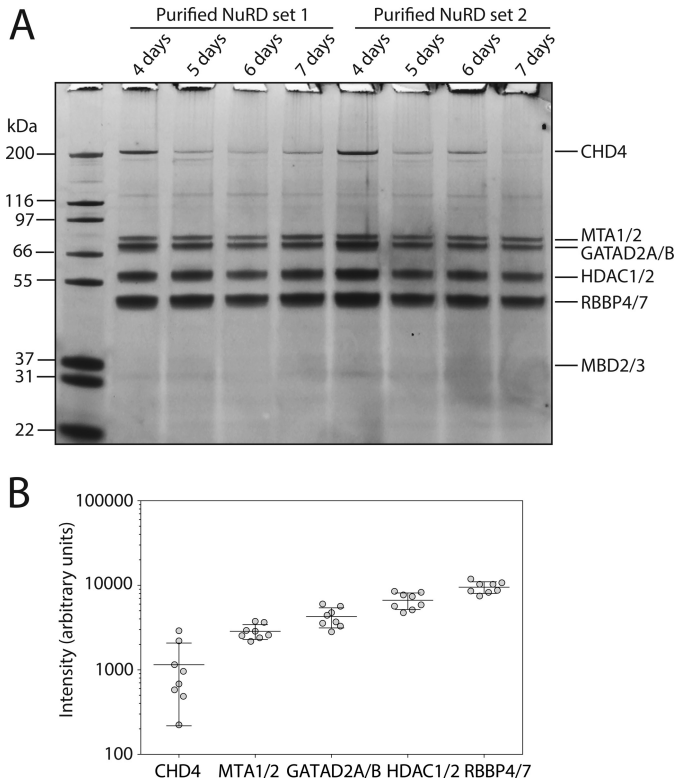

FIGURE 1. **NuRD purifies from MEL cells as +CHD4 and −CHD4 species.** *A*, SDS-PAGE showing the core components of the NuRD complex purified using FOG1 affinity chromatography. Comparison of intensities reveals that the relative amount of CHD4 varies substantially from lane to lane. In particular, culture time (number of days) appears to affect the amount of CHD4 associated with NuRD. *B*, SYPRO-Ruby-stained band intensities from the gel in *A* were quantified using the ImageJ software package. The data from all eight pulldowns are shown (*gray dots*). The mean values are depicted by the *middle black lines*, and the *ends* of the *whiskers* depict the standard deviation for a given protein. The large standard deviation of intensities for CHD4, relative to the other bands, suggests that CHD4 occupancy in the NuRD complex is highly variable and does not track together with the other components.

In these purifications, we always observe the following proteins: MTA1/2/3, GATAD2A/B. HDAC1/2, RBBP4/7, and MBD3. We also observe CHD4 but find that the amount of CHD4 is quite variable, compared with the other subunits. Fig. 1 shows that although the relative amounts of MTA, GATAD2, HDAC, and RBBP family subunits are quite consistent between different NuRD preparations, the amount of CHD4 varies dramatically (note that MBD3 stains poorly). In some cases, little or no CHD4 was observed (*e.g. right-hand lane* in Fig. 1*A*). Gel image quantification show large variations in intensity for CHD4, of the order of several hundred percent, relative to other NuRD components (Fig. 1*B*). This observation led us to propose that a stable NuRD-type complex can form in the absence of CHD4. We named this assembly the nucleosome deacetylase complex (NuDe).

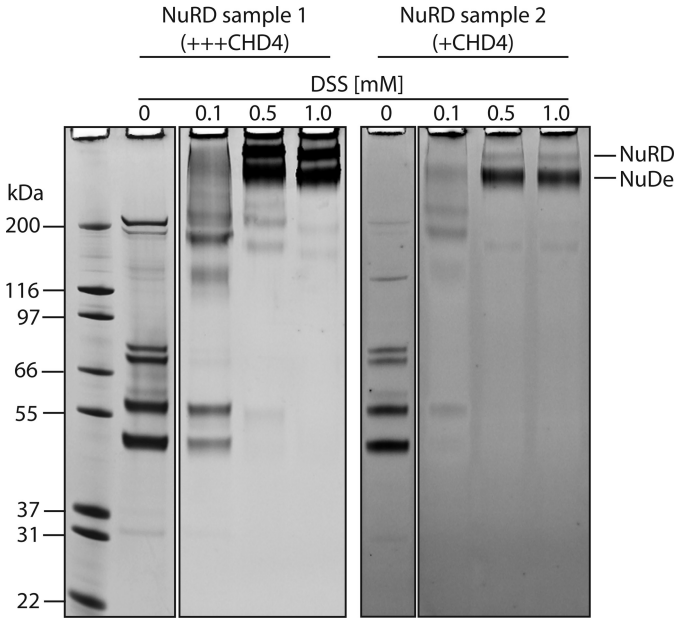

FIGURE 2. **Cross-linking of purified NuRD yields two distinct bands.** When FOG1 affinity purifications of NuRD are cross-linked using at least 0.5 mM disuccinimidyl suberate (*DSS*), two distinct high molecular weight bands are observed. When a sample with low quantities of CHD4 is cross-linked (NuRD sample 2, *right panel*), the intensity of the *upper* cross-linked band is concomitantly reduced. This suggests that the *upper* cross-linked band is the CHD4-containing NuRD complex, whereas the *lower* cross-linked band is the NuDe complex.

To investigate this observation further, we performed *in vitro* chemical cross-linking of the NuRD complex purified by FOG1 affinity chromatography. Fig. 2 (*left-hand gel*) shows clearly that the addition of the cross-linker disuccinimidyl suberate to our NuRD complex results in two distinct high molecular weight bands that run into the gel (and are therefore unlikely to represent nonspecifically cross-linked multimers). Cross-linking of a separate preparation (*right-hand gel*) that contains substantially less CHD4 (judging from the pre-cross-linked lane) shows the same two bands but with quite different relative intensities: the higher molecular weight band is of much lower intensity, consistent with the formation of a complex lacking CHD4. Blue native PAGE of the affinity-purified complex (without cross-linking) revealed two major bands at ~900 and ~720 kDa (Fig. 3*A*). The apparent mass difference is consistent with the molecular mass of CHD4 (218 kDa).

We next sought to determine the composition of these complexes by running the blue native gel lane from Fig. 3*A* in a reducing SDS-PAGE as a second dimension. As shown in Fig. 3*B*, the 900-kDa band has bands visible for all components of the NuRD complex. In contrast, the 720-kDa band yielded all components except for CHD4. The same conclusion is reached when the purified complex (bound to fluorescein-labeled FOG1(1–15)) is subjected to sucrose density gradient ultracentrifugation; fluorescent signals corresponding to NuDe and NuRD were observed at two distinct positions in the gradient (Fig. 4*A*). SDS-PAGE analysis of the gradient fractions (Fig. 4*B*) in combination with dot blot analysis of the fractions (Fig. 4*C*) confirms the existence of the lighter NuDe and the heavier NuRD complexes. Finally, direct mass spectrometric analyses of gel bands cut from the blue native PAGE (from Fig. 3*A*) and digested with trypsin confirmed the presence of all components of the NuRD complex in the 900-kDa band, whereas the 720-kDa band lacked CHD4 but contained all other components with similar levels of sequence coverage (Fig. 3*C*). Taken together, these complementary lines of evidence suggest that, even in the absence of CHD4, all other components of the NuRD complex can assemble into a stable entity that is likely to have the same subunit stoichiometry.

The NuDe Complex Has Robust Deacetylase Activity—The observation of two distinct complexes raises questions about the function of the smaller entity. We asked whether the NuDe complex still possessed protein deacetylase activity; inactivation of NuRD following the loss of CHD4 could serve as an effective form of functional regulation of the complex. We performed HDAC activity assays on purified NuDe complex (calculated to contain only ~1–2% NuRD). As shown in Fig. 5, the NuDe complex possesses robust deacetylase activity. When compared with the manufacturer-supplied HDAC positive control, the NuDe complex was approximately four times as active.

NuRD Can Be Reconstituted by Adding CHD4 to NuDe—The observation that CHD4 occupancy in the NuRD complex is highly variable suggests that CHD4 is not in the core of the complex but rather at the periphery. We reasoned that, if this is the case, we should be able to supplement our NuDe complex with heterologously produced CHD4 to reconstitute the full NuRD complex.

For these CHD4 supplementation experiments, we used FLAG-CHD4 transiently expressed in mammalian HEK293FT cells. Despite its large size (~218 kDa), we were able to express and purify CHD4 (Fig. 6*A*). When we mixed HEK293FT nuclear extracts containing FLAG-CHD4 with MEL cell nuclear extracts prior to incubation with the FOG1-immobilized beads, we observed that the occupancy of CHD4 was increased in the complex (Fig. 6*B*). To calculate the proportion of CHD4 in our NuDe/NuRD preparations, we sought to account for differences between NuRD subunits in their gel staining properties. We first determined the ratio of NuDe to NuRD in each fraction taken from our sucrose gradient purifications of MEL cell-derived complex by fitting each fluorescence trace (from three independent sucrose gradients; *e.g.* as shown in Fig. 4*A*) to a sum of two Lorentzians (Fig. 6*C*). Fig. 6*D* shows the calculated molar ratio of NuRD to NuDe across different fractions. The NuRD:NuDe ratio was as high as ~80% in some fractions.

We then measured the intensities of each NuRD subunit band in Sypro-stained SDS-PAGEs of selected sucrose gradient fractions. To derive a scaling factor to account for the gel staining properties of each subunit, we took into account the NuRD:NuDe ratio calculated for each of these fractions above and also the number of copies of each subunit in the complex (derived from published stoichiometry data on the NuRD complex (31, 32)). Fig. 6*E* shows the gel stain scaling factors for each NuRD subunit, relative to a value of 1 set for HDAC1/2. Using these values to assess our CHD4-supplemented NuDe samples, we estimate that the "loading" of CHD4 increased from 22 to 63% following supplementation. We note that an additional band at ~66 kDa co-elutes with our NuRD complex (Fig. 6*B*). This pro-

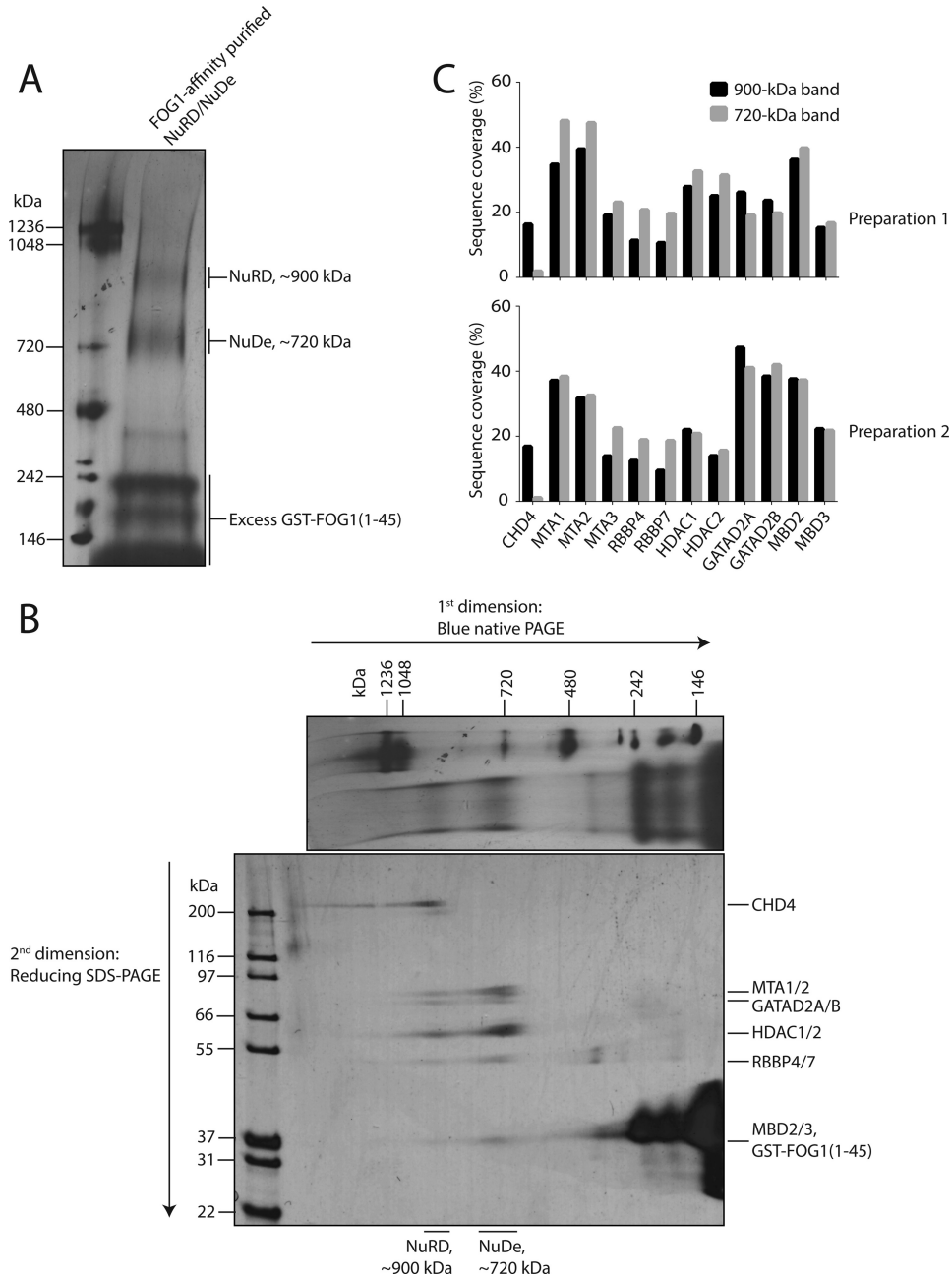

FIGURE 3. **The NuRD and NuDe complexes migrate as separate complexes under native conditions.** *A*, blue native PAGE of the FOG1 affinity-purified NuDe/NuRD complexes. Two major bands are observed at 900 and 720 kDa, corresponding to NuRD and NuDe, respectively. *B*, with reducing SDS-PAGE as the second dimension, two-dimensional blue native SDS-PAGE of a NuDe/NuRD purification shows that the 900-kDa NuRD band has CHD4, whereas the 720-kDa NuDe band does not. Both bands contain all other NuRD components. *C*, approximate quantification of NuRD components by mass spectrometry. The 900-kDa NuRD and 720-kDa NuDe gel bands from blue native PAGE (Fig. 3*A*) were cut out, digested with trypsin, and then subjected to mass spectrometric analysis. The resulting protein sequence coverage for each protein from LC-MS/MS is shown, suggesting that the 720-kDa band does not contain significant quantities of CHD4. The results from two independent NuRD preparations are shown.

tein has been identified as heat shock 70-kDa protein 1 via tandem mass spectrometry and is a commonly known contaminant in affinity purifications (39). This contaminant band is not present when we instead supplement our NuDe/NuRD complex with FLAG tag-purified CHD4.

To confirm that addition of exogenous CHD4 created a functionally intact NuRD complex, we assessed the nucleosome remodeling activity of our CHD4-supplemented NuDe/NuRD preparations (by direct addition of purified CHD4 to NuDe/NuRD) against unsupplemented NuDe/NuRD preparations and purified CHD4 only. Real time FRET-based nucleosome repositioning assays similar to those described by Yang *et al.* (40) were carried out. We have previously used this assay to assess CHD4 nucleosome remodeling activity (41). Briefly, histone octamers containing an Alexa Fluor 488-labeled histone H2A cysteine mutant (T120C) were assembled on 0W47 DNA (that is, Widom nucleosome positioning sequence flanked by 0 and 47 bp upstream and downstream, respectively) labeled with the dark quencher BHQ1, generating asymmetric end-positioned nucleosomes. In these nucleosomes, the proximity of the

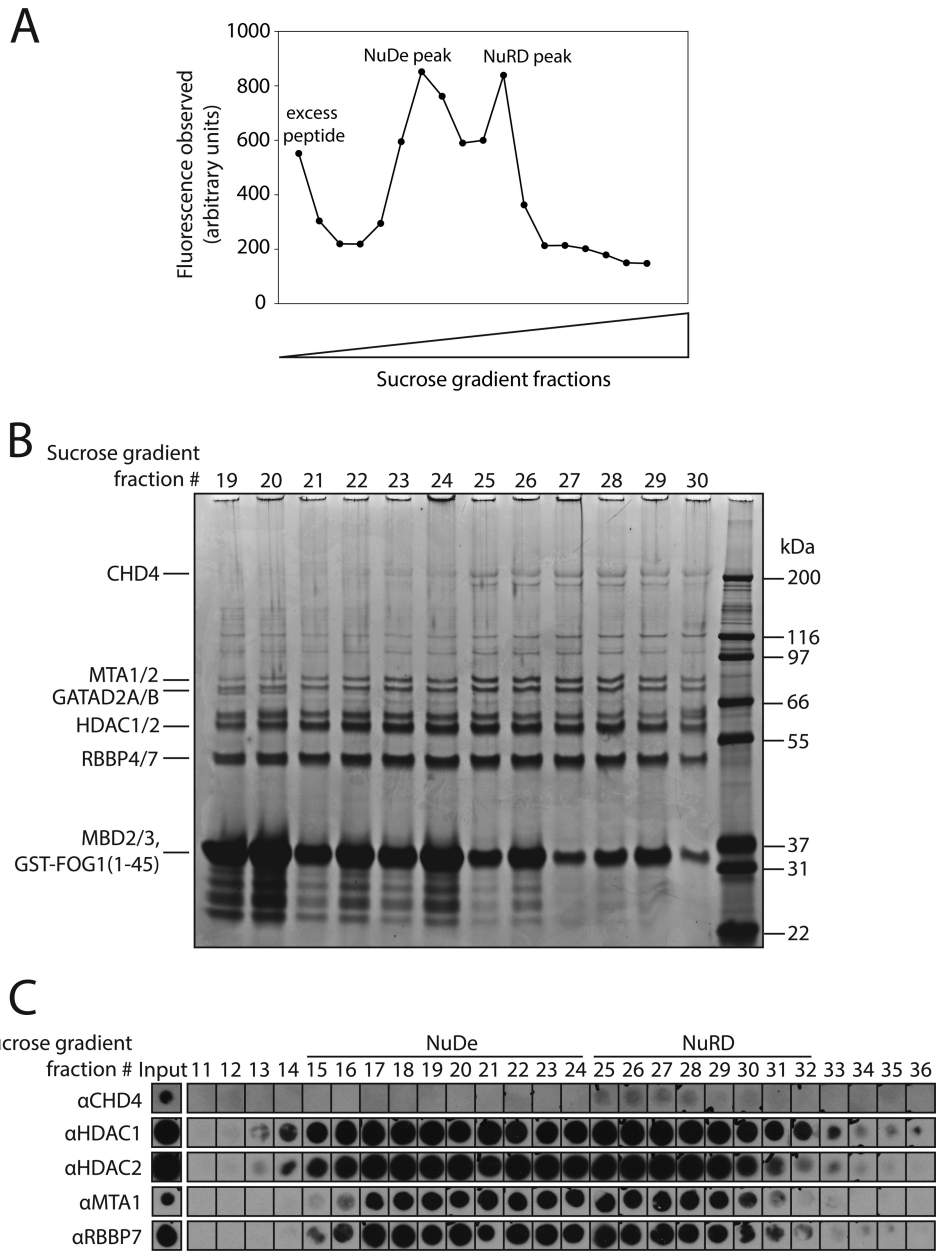

FIGURE 4. **Sucrose density gradient ultracentrifugation analyses of NuDe/NuRD purifications yield two high molecular weight complexes.** *A*, the fluorescence of sucrose gradient fractions close to where the NuDe/NuRD complex equilibrates is plotted against depth in the gradient. Two distinct fluorescent peaks corresponding to NuDe and NuRD were observed. *B*, SDS-PAGE analysis of sucrose gradient fractions. Using the presence of CHD4 as a guide, the NuDe complex is observed to elute in earlier fractions (~19–24), whereas the NuRD complex elutes later (~25 onwards). *C*, dot blot analysis of sucrose gradient fractions. Consistent with the SDS-PAGE analysis in *B*, CHD4 is only detectable from fraction 25 onwards.

BHQ1 moiety to the Alexa Fluor 488 results in strong quenching of Alexa Fluor 488 fluorescence. Any movement of the BHQ1 away from the Alexa Fluor 488 dye, such as that arising from ATP-dependent repositioning by a remodeling enzyme, results in a robust increase in fluorescence that can be monitored in real time. Supplementation of a NuRD preparation containing a substoichiometric quantity of endogenous CHD4 (NuDe/NuRD) with recombinant FLAG-CHD4 (Fig. 7, *A*, *solid gray line*, and *B*) gives rise to a synergistic increase in ATP-dependent remodeling activity; that is, the activity of NuDe/NuRD + CHD4 top-up is higher than the summed activity of NuDe/NuRD-only and CHD4-only (Fig. 7, *A*, *dotted gray line*, and *B*). Similar results were obtained when classical gel-based nucleosome repositioning assays were performed; a synergistic increase in ATP-dependent remodeling activity was observed for the NuDe/NuRD sample topped-up with CHD4 (Fig. 7*C*, *lanes 3–5 versus lanes 6–8*). As a control, we show that when an unrelated protein such as BSA is added to recombinant CHD4, no enhancement of CHD4 remodeling is observed; in fact, CHD4 activity is reduced by ~20–65% following the addition of 75 nM BSA (Fig. 7*D*, *black lines versus gray lines*). Note that the total mass of BSA used in this assay was the same as the total mass of NuDe/NuRD used in Fig. 7 (*A*—*C*), suggesting that the synergistic effect of NuDe/NuRD on CHD4 remodeling activity is not due to nonspecific carrier protein effects.

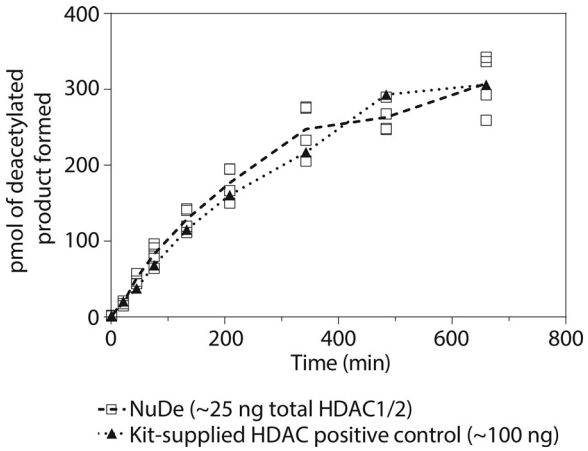

FIGURE 5. **The NuDe complex has robust deacetylase activity.** Deacetylase activity was measured for four NuDe/NuRD preparations with a low proportion of CHD4/NuRD (*white squares*; mean values depicted by *dashed line*). Through the course of the deacetylase activity assay, samples were taken at nine time points, developed, and measured for product fluorescence. The amount of deacetylase activity observed for the HDAC-positive control (supplied by the assay kit's manufacturer) is indicated by the *black triangles* and *dotted line*.

These data reinforce the observation that native NuRD preparations from MEL cells carry substoichiometric amounts of CHD4. In turn, this observation implies that CHD4 lies at a boundary rather than a core location in the NuRD complex. Furthermore, it is apparent that the nucleosome remodeling activity of CHD4 is positively regulated by other subunits of the NuRD complex.

Discussion

Our Understanding of Remodeler Structure Is Still Limited—Chromatin remodeling complexes play a variety of essential roles in the regulation, replication, and expression of the genome. Their dysregulation is closely linked with a variety of pathologies, most notably cancer (23, 42, 43). However, the multisubunit nature of these complexes, combined with the complexity of their substrate, has hampered efforts to understand the biochemistry underlying their function. The structure of these complexes will naturally form the basis for their function, and so an appreciation of the architecture of chromatin remodelers will underpin our understanding of their activity.

Until very recently, only very low resolution structural information was available for any multisubunit remodeling complex. Several structures of RSC from EM data (at ~25–37 Å) show a central cavity that seems to be occupied by an added nucleosome (9, 10, 13). SWI/SNF cryo-EM data (23 Å) suggest a roughly spherical structure with a surface cavity that is proposed to accommodate a nucleosome (11), and an EM study of the human PBAF complex (12) (~43–50 Å) also suggests a possible nucleosome binding site. These studies are a valuable first step, but in no case could subunits of the complex be placed with any confidence.

The highest resolution analyses of multisubunit chromatin remodelers have come recently in studies of two related complexes. Tosi *et al.* (16) built a model from cryo-EM data of the yeast INO80 complex to a resolution of ~17 Å. The model (Fig. 8*A*) shows a distinct unit with rough 6-fold symmetry that is consistent with two stacked hexamers of the ATPase Rvb1/2. Judging from the EM model and also cross-linking data, this unit is connected only to the Snf2 family remodeling protein Ino80, which in turn is connected to Arp5, Nhp10, and Ies2 modules. An Arp8 module, which appears to display substantial mobility, is distally connected to Nhp10. Although EM data (~28 Å) for the related SWR1 complex, also from yeast, unexpectedly yielded quite a different model (14), a clear commonality between the two models was the scaffolding role played by the Snf2 family remodeling subunit.

CHD4 Is a Peripheral Component of NuRD—The NuRD complex is perhaps the most enigmatic of the major chromatin remodeling complexes, from a structural and biochemical perspective. The lack of structural data is due in large part to the restriction of NuRD to multicellular animals and an apparent inability to reassemble the NuRD complex from recombinantly expressed subunits.

The literature shows that CHD3, CHD4, and CHD5 can all act as the remodeling subunit of the NuRD complex. These proteins share a topology that includes two PHD domains, two chromodomains, an ATPase domain, and a C-terminal region of unknown structure. CHD3 and CHD4 are broadly expressed, whereas CHD5 is present at significantly higher levels in the brain (44). Drawing from biochemical data and in common with the INO80/SWR1 complexes, it is widely held that the CHD remodeler acts as a scaffold around which the NuRD complex is assembled (18, 33–35).

Our data show clearly that the converse is true: that CHD4 is a peripheral component of the complex. HDAC, MTA, GATAD2, RBBP, and MBD proteins can assemble into a stable complex in the absence of a CHD4 family member. This NuDe complex, like NuRD, can be purified via its affinity for the co-regulator FOG1 and subsequently sucrose gradient centrifugation. We also show that the NuDe complex displays unimpaired deacetylase activity. The full NuRD complex can be reconstituted through the addition of recombinant CHD4, and this complex displays ATP-dependent nucleosome remodeling activity that exceeds the activity of CHD4 alone. Hence, the observations that the NuDe complex has functional deacetylase activity and that CHD4 can be supplemented to NuDe to make NuRD, combined with already published data that the MBD2 and MBD3 subunits are mutually exclusive (5), strongly make the case that the NuRD complex is relatively modular. That is, a core module built around HDAC, MTA, and RBBP subunits carries histone recognition and modification functions, MBD subunits contribute DNA targeting ability, and CHD3/4/5 carries out the remodeling. Such a model is also consistent with data showing that MBD2 binds directly to the HDAC-MTA core complex (45). This idea also raises the possibility that there are other modules that we have yet to learn about, considering that the NuRD complex has been reported to associate with a number of other proteins, including DOC1, ZMYND8, ZNF592, and LSD1 (32, 46, 47).

How is CHD4 recruited to the NuDe complex? Chemical cross-linking data from the Vermeulen laboratory revealed cross-links between CHD3/4 (both were observed in their data) and both GATAD2A/B and MTA1/2 (31). In contrast, no

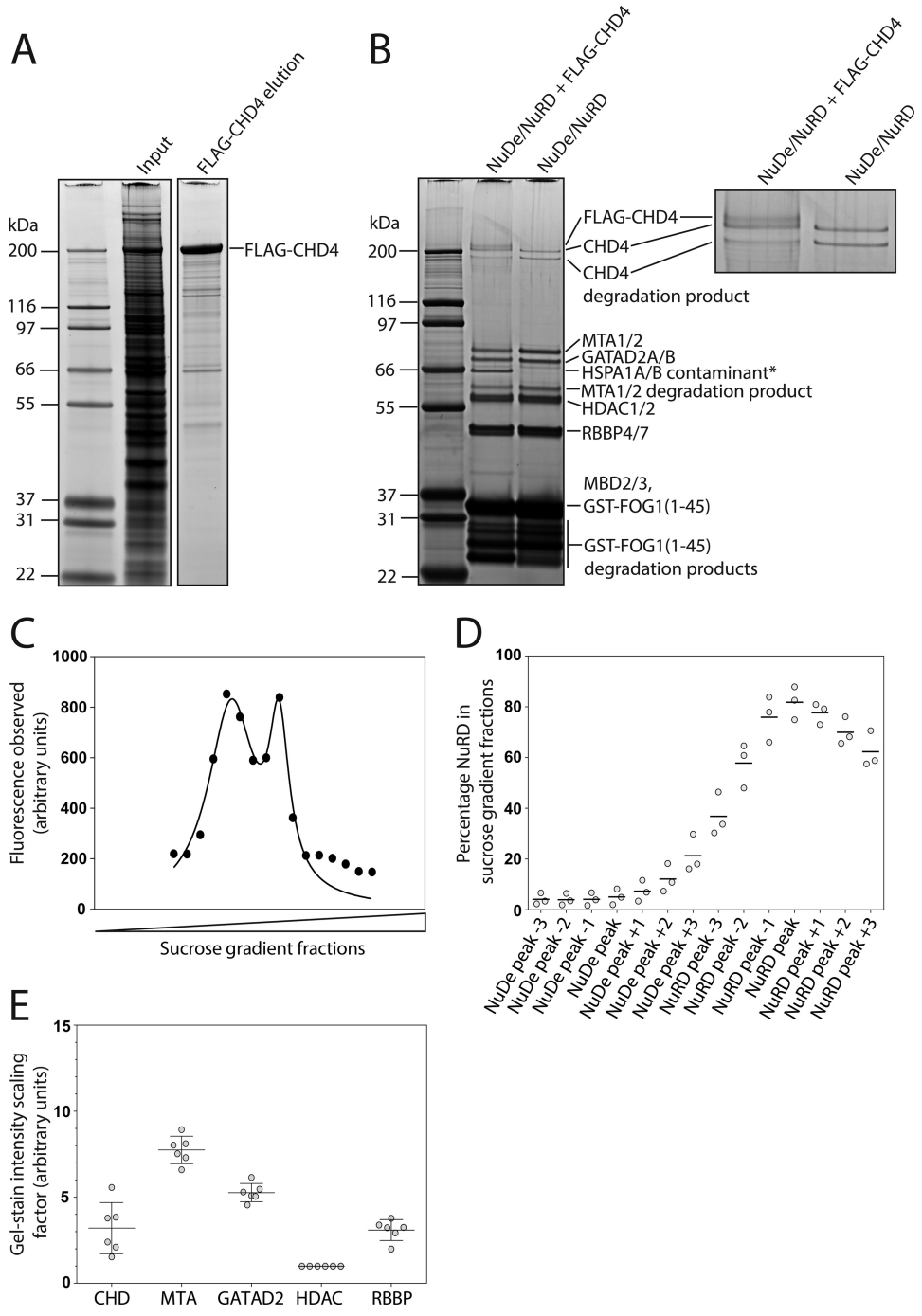

FIGURE 6. **NuDe can be supplemented with exogenous recombinant FLAG-CHD4.** *A*, SYPRO-Ruby-stained SDS-PAGE showing expression and purification of FLAG-CHD4 from HEK293FT cells. Gel lanes (from the *left*) show molecular weight markers, total soluble fraction from lysed cells expressing FLAG-CHD4, and purified FLAG-CHD4. *B*, SYPRO-Ruby-stained SDS-PAGE showing that NuDe/NuRD preparations can be supplemented with recombinant FLAG-CHD4. Gel lanes (from the *left*) show molecular weight markers, FOG1 affinity purification of NuDe/NuRD supplemented with FLAG-CHD4 (by mixing MEL cell nuclear extract with FLAG-CHD4-expressed HEK293FT nuclear extract), and FOG1 affinity purification of NuDe/NuRD without supplementation. The 66-kDa band (denoted with an *asterisk*) in the CHD4-supplemented NuDe/NuRD purification is the common contaminant HSPA1A/B. Shown on the *right* of this panel is an enlarged image of the 200-kDa region of the gel. Three bands corresponding to FLAG-CHD4, native CHD4, and a degradation product of CHD4 can be seen. *C*, the fluorescence plots from the NuDe/NuRD sucrose gradient fractions were peak-fitted using the sum of two Lorentzian curves. The *dots* represent the actual fluorescence measured, whereas the *solid line* depicts the fitted curve. Data from three independent sucrose gradients were used. A representative plot is shown here. *D*, using the best fit values from *C*, the molar ratio of NuRD to NuDe was calculated across different sucrose gradient fractions. Data from three independent sucrose gradients are shown as *open circles*, and the mean values are depicted by *black lines*. *E*, gel stain scaling factors for various NuRD subunits relative to HDAC1/2. To derive gel stain scaling factors for various NuRD subunits, densitometry data of each NuRD subunit band in SYPRO-Ruby-stained sucrose gradient gels were combined with pre-existing data on the NuRD stoichiometry and the NuRD:NuDe ratios in *D*. Six sucrose gradient fraction samples (*gray circles*) were used for the calculation. Mean values are depicted by the *middle black lines*, and the *ends* of the *whiskers* show the standard deviation.

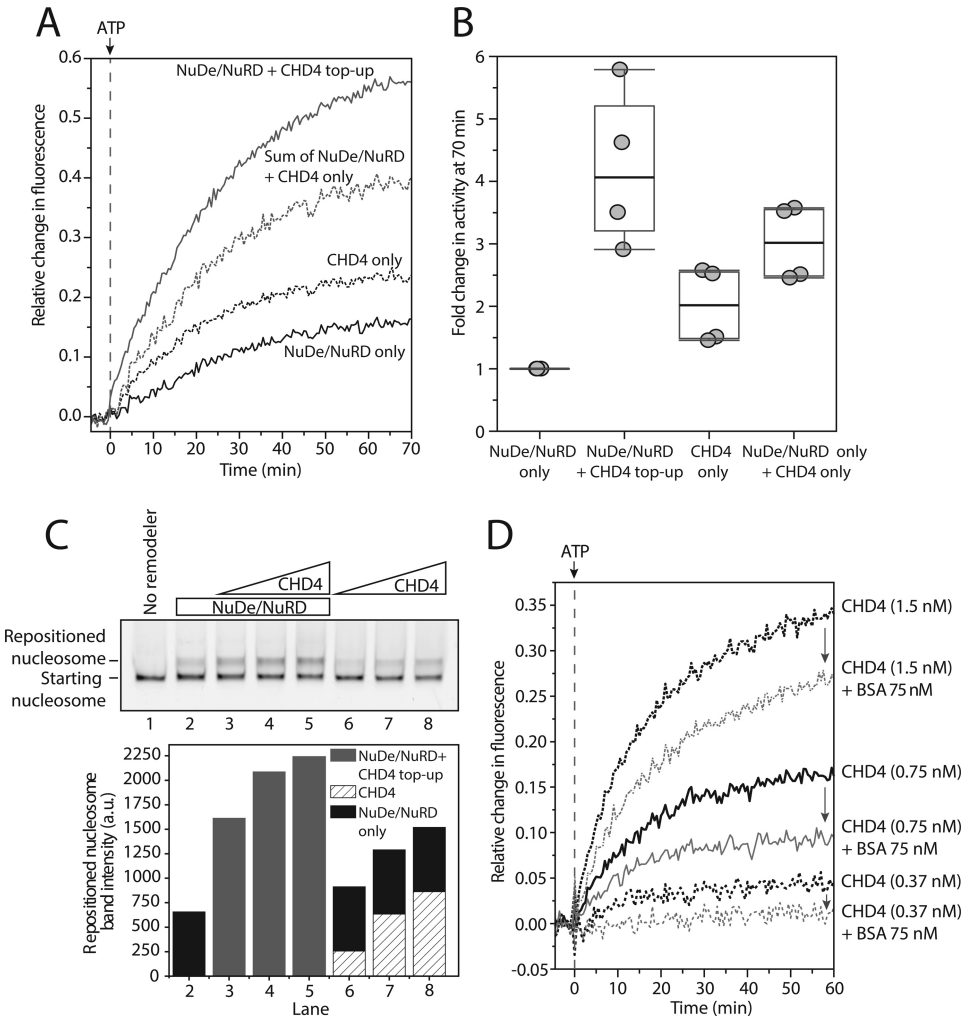

FIGURE 7. **Functional NuRD complex can be reconstituted from NuDe plus recombinant CHD4.** *A*, real time nucleosome repositioning traces for NuDe/NuRD (5 ng/μl; ~6.25 nM) in the absence (NuDe/NuRD only; *solid black line*) or presence (NuDe/NuRD + CHD4 top-up; *solid gray line*) of recombinant CHD4 (0.75 nM). Repositioning activity of CHD4 alone (0.75 nM; *dotted black line*) and a theoretical trace representing the sum of the NuDe/NuRD-only and CHD4-only data (*dotted gray line*) are also shown. The NuDe/NuRD + CHD4 top-up trace (*solid gray line*) is always higher than the sum of NuDe/NuRD only + CHD4 only trace (*dotted gray line*), suggesting that CHD4 remodeling activity is enhanced when it is part of the NuRD complex. The *vertical dashed line* indicates the addition of ATP to the reaction. *B*, quantitation of the relative differences in nucleosome repositioning activity (as shown in *A*). Total signal change after 70 min was determined, and the fold change in activity relative to the NuDe/NuRD-only sample was calculated. The NuDe/NuRD only + CHD4 only data points were obtained by summing the NuDe/NuRD-only and CHD-only data. Data from four independent experiments are shown (*gray dots*), the median values are depicted by the *gray bars* within the boxes, the *bottoms* and *tops* of the *boxes* represent the first and third quartile, and the *ends* of the *whiskers* depict the minimum and maximum values of all the data. *C*, gel-based nucleosome repositioning assay for NuDe/NuRD (5 ng/μl; ~6.25 nM) in the absence (NuDe/NuRD only; *lane 1*) or presence (NuDe/NuRD + CHD4 top-up; *lanes 2–5*)) of recombinant CHD4 (0.37, 0.75, and 1.5 nM). Repositioning activity of CHD4 alone (0.37, 0.75, and 1.5 nM) are shown in *lanes 6–8*. In the *lower panel*, in-gel fluorescence of the repositioned nucleosome band was quantified. The NuDe/NuRD only samples are depicted as *black bars*, and the NuDe/NuRD + CHD4 top-up samples are depicted as *gray bars*, whereas the CHD4 only samples are depicted by *hatched bars*. In all instances tested, a synergistic effect on CHD4 remodeling activity was observed in the presence of NuDe/NuRD. *D*, real time nucleosome repositioning traces for recombinant CHD4 (0.37, 0.75, and 1.5 nM) in the absence (*black solid and dashed lines*) or presence of bovine serum albumin (5 ng/μl; 75 nM; *gray solid and dashed lines*). The *vertical dashed line* indicates the addition of ATP to the reaction. The data show that at all concentrations of CHD4 tested, remodeling activity of CHD4 is decreased by ~20–65% in the presence of BSA (*gray arrows*), suggesting that the synergistic effect of NuDe/NuRD on CHD4 remodeling activity observed in *A–C* is specific and not due to carrier protein effects.

cross-links were observed from CHD3/4 to any of the subunits HDAC1/2, RBBP4/7, or MBD2/3. The four CHD-MTA cross-links ($CHD3_{K1067}$-$MTA2_{K639}$, $CHD4_{K1390}$-$MTA2_{K686}$, $CHD4_{K266}$-$MTA1_{K532}$, and $CHD4_{K266}$-$MTA2_{K532}$) all map to the C-terminal half of MTA1/2, which is predicted to be largely disordered. Interestingly, the first two of these cross-links implicate residues in MTA1/2 that lie adjacent to the RBBP4/7 binding motif of those proteins (30), suggesting that this C-terminal portion of the MTA proteins might perform a scaffolding function to some degree. Similarly, the other proteins to which CHD3/4 displayed cross-links, GATAD2A/B, are predicted to be largely disordered. The function of GATAD2A/B is completely unknown, although a small region does form a coiled-coil with MBD2/3 (29). It is tempting to speculate that these predicted disordered regions, which are quite extensive in length (*e.g.* ~500 of 633 residues of GATAD2A), might undergo folding-upon-binding transitions to tether a CHD remodeler to the NuDe complex. In this context it is notable that the server D2P2 (48) predicts that the sequence of GATAD2A contains a large number of predicted molecular recognition features: short sequences that are likely to act as protein-binding motifs (49), adding credence to the idea that it can act as a CHD recruitment module.

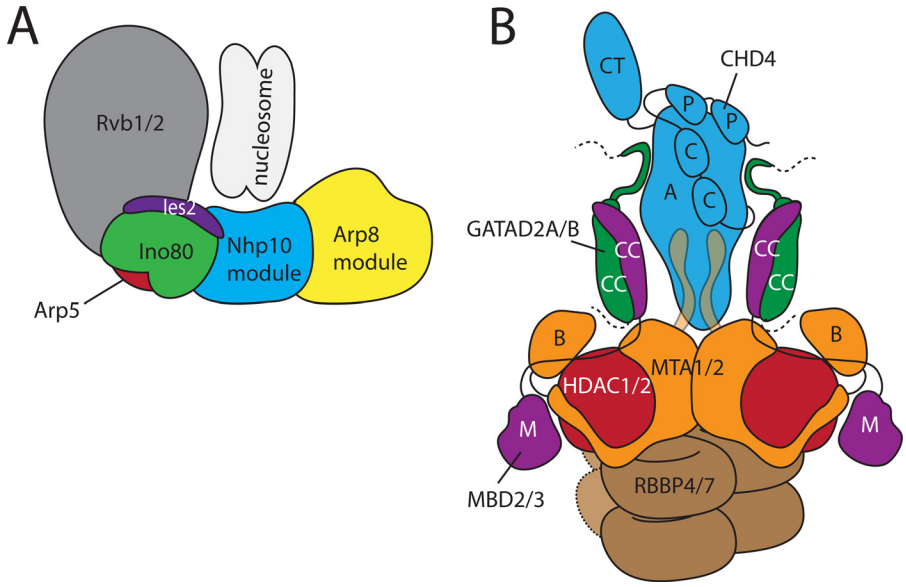

FIGURE 8. **Cartoon representations of the NuRD and INO80 complexes.** *A*, model of the INO80 complex (adapted from Ref. 16). Each module, which comprises one or more proteins, is indicated. *B*, cartoon of the NuRD complex. The cartoon is based on the published structural, stoichiometry, and cross-linking data discussed in the text. *Brown*, RBBP4/7; *red*, HDAC1/2; *orange*, MTA1/2/3; *purple*, MBD3; *dark blue*, GATAD2A/B; *cyan*, CHD3/4/5. *B*, BAH domain; *M*, methyl-binding domain; *CC*, coiled-coil; *P*, PHD domain; C, chromodomain; *CT*, C-terminal domain; *A*, ATPase domain.

Stoichiometry data for the NuRD complex, also from the Vermeulen laboratory, have suggested two slightly varying subunit ratios (RBBP:MTA:GATAD2:HDAC:MBD:CHD) of ~6:3:2:1:1:1 (32) and 5–6:2–3:2–3:2:2:1 (31). The latter data are more consistent with the stoichiometries observed in the structures of the HDAC1-MTA1 and MBD3-GATD2A subcomplexes and imply that the complex contains a single CHD subunit that is held in place by two GATAD2A and two MTA subunits. These interactions are represented in Fig. 8*B*, which shows a cartoon of the complex based on the published structural and stoichiometric data. The regions with known structures are represented approximately to scale, whereas the sequence predicted to be disordered is generally not shown.

All of the proteins in the NuRD complex have the capacity to interact with some component of the nucleosome. The RBBPs have been shown to have histone H3 and H4 binding properties (37, 50); MTA1/2/3 contain BAH domains, which have also been shown to recognize histone H3 (51); MBD2/3 have DNA-binding domains that have been shown to bind methylated and hydroxymethylated DNA (6, 7), respectively; GATAD2A/B contain GATA-type zinc fingers, which commonly act as DNA-binding domains, and the enzymes CHD3/4/5 and HDAC1/2 have nucleosomes as their substrates. It is notable that a cross-link is observed between the MTA2 BAH domain and the MBD3 MBD domain, juxtaposing these histone and DNA-binding domains (Fig. 8*B*). It follows that the overall conformation of the NuRD complex will need to allow these interactions to all take place, although not necessarily simultaneously, and the complex will not necessarily only interact with a single nucleosome at a given time.

Does CHD4 Have NuRD-independent Functions?—The peripheral location of CHD4 in the NuRD complex could allow relatively straightforward addition and removal of CHD4 from the complex. Shuttling of this type might constitute a mechanism by which the activity of NuRD can be regulated. Similarly, it might provide a means by which CHD4 can carry out NuRD-independent functions. It has recently been suggested, for example, that roles of CHD4 in the DNA damage response and in cell cycle progression might in some cases be independent of NuRD (19, 41). However, examination of published data does not reveal any examples in which NuRD-independent activity has clearly been demonstrated. Nevertheless, one recent study does demonstrate that an interaction between CHD4 and the histone methyltransferase Ezh2, a core component of the Polycomb repression complex, is essential for the ability of Polycomb to repress the gene GFAP during astroglial differentiation (52). In an Ezh2-directed affinity purification experiment, CHD4 was detected by Western blot, but neither MTA2 nor MBD3 were observed, suggesting that this interaction does not involve the full NuRD complex. It is notable that the Polycomb complex does contain RBBP4/7, and it is possible that CHD4-RBBP4/7 contacts are a feature of both the NuRD and the CHD4-Polycomb interactions.

The extent to which CHD4 acts independently of NuRD is therefore still very much an open question. The data described here demonstrate that severing of the NuRD-CHD4 link through engineered mutations should be possible without complete disassembly of the NuRD complex and that the remaining NuDe complex could still act to modify histone structure. Targeted disruption of these interactions will permit a more rigorous delineation of the division between the different possible modes of CHD4 activity. Similarly, the ability to reconstitute the NuRD complex in a straightforward manner with recombinant CHD4 opens the door to a detailed mechanistic analysis of CHD4- and NuRD-mediated chromatin remodeling.

Experimental Procedures

Cell Culture—MEL cells were cultured as described previously (38), with the exception that the medium used for large scale grow-ups was also supplemented with 50% Ham's F-12

nutrient mix. Briefly, 10–20-ml seed cultures were maintained in DMEM (with 4.5 g/liter D-glucose and 110 mg/liter sodium pyruvate) supplemented with 5% (v/v) FBS, 50 units/ml penicillin and 50 μg/ml streptomycin and grown at 37 °C, 5% CO_2. For large scale grow-ups, 250-ml batches of fresh DMEM supplemented with 50% (v/v) Ham's F-12 nutrient mix and 5% (v/v) FBS were each inoculated with 2×10^6 cells. The cells were harvested at a density of $\sim 1 \times 10^6$ cells/ml by centrifugation (300 *g*, 5 min). The typical yield is ~1 g (wet weight) of cells/liter of culture. The cells were washed twice in PBS, frozen in liquid nitrogen, and stored at −80 °C until use. All materials were purchased from Gibco.

FOG1 Affinity Pulldown—Affinity resin preparation, nuclear extract preparation, and FOG1 affinity pulldowns were performed as described previously (36, 38). Briefly, for StreptagII-FOG1(1–15), synthesized peptides were dissolved in NuRD binding buffer (50 mM HEPES-KOH, 150 mM NaCl, 1% (v/v) Triton X-100, 1 mM DTT, 1× cOmplete® protease inhibitor (Roche), pH 7.4) and incubated with pre-equilibrated Streptactin beads for 2 h at 4 °C. The beads were then washed with 20 column volumes (CV) of NuRD binding buffer and used for pulldown experiments.

For GST-FOG1(1–45), *Escherichia coli* BL21(DE3) cells containing overexpressed GST-FOG1(1–45) were lysed via sonication in GST binding buffer (50 mM Tris, 150 mM NaCl, 0.1% β-mercaptoethanol, 0.5 mM PMSF, 0.1 mg/ml lysozyme, 10 μg/ml DNase I, pH 7.5) and clarified via centrifugation (≥16,000 × *g*, 20 min, 4 °C). The cleared supernatant was then incubated with pre-equilibrated glutathione-Sepharose 4B beads (GE Healthcare) for 1 h at 4 °C. The beads were then washed in GST wash buffer (20 CV, 50 mM Tris, 500 mM NaCl, 1% (v/v) Triton X-100, 1 mM DTT, pH 7.5) and then NuRD binding buffer (10 CV). The beads were then used for pulldown experiments. MEL cell nuclear extracts were prepared by incubating the thawed cell pellets with hypotonic lysis buffer (5 ml/g of cells; 10 mM HEPES-KOH, 1.5 mM $MgCl_2$, 10 mM KCl, 1 mM DTT, cOmplete® protease inhibitor, pH 7.9) for 20 min at 4 °C. IGEPAL® CA-630 was then added (final concentration, 0.6% v/v), and the cells were then further incubated for 10 min. The mixture was then vortexed for 10 s and then centrifuged (3,300 × *g*, 5 min). The cytoplasmic supernatant was discarded, and the nuclear pellet was gently washed once with lysis buffer (+0.6% (v/v) IGEPAL® CA-630).

The washed nuclear pellet was resuspended in NuRD binding buffer (3 ml/g of cells), then lysed by sonication, and incubated on ice for 30 min to allow the chromatin to precipitate. The nuclear extract was then clarified via centrifugation (≥16,000 × *g*, 20 min, 4 °C), and the cleared supernatant was incubated with Streptavidin beads (a preclearing step for FOG1(1–15) peptide affinity purification) before incubating with the above FOG1 affinity resins overnight at 4 °C. Postincubation, the nuclear extract was then washed with 20 CV of NuRD wash buffer 1 (50 mM HEPES-KOH, 500 mM NaCl, 1% (v/v) Triton X-100, 1 mM DTT, pH 7.4) and then 10 CV of NuRD wash buffer 2 (50 mM HEPES-KOH, 150 mM NaCl, 0.1% (v/v) Triton X-100, 1 mM DTT, pH 7.4). Captured proteins were eluted with either StreptagII-FOG1(1–15) elution buffer (10 mM biotin, 50 mM HEPES-KOH, 150 mM NaCl, 0.1% Triton X-100, 1 mM DTT, pH 8.2) or GST-FOG1(1–45) elution buffer (50 mM reduced glutathione, 50 mM HEPES-KOH, 150 mM NaCl, 0.1% Triton X-100, 1 mM DTT, pH 8.0) for 30 min at 4 °C. This elution step was repeated at least twice to ensure complete elution.

Disuccinimidyl Suberate Cross-linking—Cross-linking reactions were initiated by the direct addition of disuccinimidyl suberate (25 mM stock dissolved in anhydrous dimethylformamide) to the purified NuRD-NuDe complex at a final concentration of 0.1, 0.5, or 1 mM. The samples were then incubated at 37 °C for 30 min and quenched with 100 mM NH_4HCO_3 (final concentration, 50 mM) and further incubated at 37 °C for 20 min.

Blue Native PAGE and Two-dimensional Blue Native SDS-PAGE—Purified NuRD/NuDe samples were prepared in 1× NativePAGE sample buffer (50 mM Bis-Tris, 6 N HCl, 50 mM NaCl, 10% (w/v) glycerol, 0.001% (w/v) Ponceau S, pH 7.2) and loaded onto 3–12% NativePAGE™ Novex® Bis-Tris gels. The gels were run at a constant voltage of 100 V for 1 h then at 250 V until the dye front migrated to the end of the gel using 1× NativePAGE running buffer (50 mM Bis-Tris, 50 mM Tricine, pH 6.8) at the anode and the "light blue" buffer (50 mM Bis-Tris, 50 mM Tricine, 0.002% (w/v) Coomassie® G-250, pH 6.8) at the cathode. The apparent molecular masses of protein complexes were estimated by comparison with the NativeMark® high molecular mass markers. For two-dimensional blue native SDS-PAGE analysis, following the first dimensional blue native PAGE separation, the blue native gel lane was excised and equilibrated in 1× SDS sample loading buffer (37 °C, 20 min). The equilibrated gel lane was then placed into a NuPAGE® Novex® 4–12% Bis-Tris gel (well separators were removed prior) and run at 180 V using 1× MES SDS-PAGE buffer.

Sucrose Density Gradient Ultracentrifugation and Dot Blots—5–35% sucrose density gradients in 50 mM HEPES-KOH, pH 8.2, and 150 mM NaCl were prepared using the Biocomp Gradient Master. Prepared gradients were left standing at 4 °C for at least 1 h prior to usage. Up to 500 μl of samples were then layered on top of each gradient and ultracentrifuged (186,000 × *g*, 4 °C, 18 h). The gradients were fractionated as 200-μl aliquots prior to further downstream analysis. When using the StreptagII-FOG1(1–15) peptide, the location of the NuRD and NuDe complexes could be determined by the fluorescence of the fluorescein moiety on the StreptagII-FOG1(1–15) peptide. Fractions from the sucrose density gradients were dot blotted and processed as previously described (38).

Mass Spectrometry—Gel bands were prepared essentially as described previously (38) with minor modifications. Briefly, gel bands were excised, shredded (53), equilibrated (50 mM NH_4HCO_3, 10 min), destained (50 mM NH_4HCO_3, 50% (v/v) CH_3CN, three or four treatments until all Coomassie® has been removed), and dehydrated (100% CH_3CN, 10 min). The dried gel pieces were then reduced (10 mM DTT, 1 h, 55 °C), alkylated (50 mM iodoacetamide, 20 min, room temperature in the dark), washed in 50 mM NH_4HCO_3 (10 min), and dehydrated in 100% CH_3CN (10 min). Trypsin (12 ng/μl) was then added to the gel pieces in an ~1:50 enzyme:substrate ratio and left to rehydrate (10 min).

The gel pieces were then topped up with 50 mM Tris, pH 8, to just cover the gel pieces. The mixture was incubated at 37 °C for

16 h. The supernatant containing the tryptic peptides were transferred to a fresh tube. The gel pieces were then treated with 50 μl each of the following solutions sequentially for 20 min each before they were removed and pooled with the overnight supernatant: (i) 0.1% (v/v) trifluoroacetic acid; (ii) 0.1% (v/v) trifluoroacetic acid, 60% (v/v) CH_3CN; and (iii) 100% CH_3CN. The pooled supernatant was then dried, resuspended in (2% formic acid), and desalted using C18 stage-tips. For LC-MS/MS, peptides were resuspended in 2% (v/v) acetonitrile, 0.5% (v/v) acetic acid and loaded onto a 20-cm × 75-μm inner diameter column packed in-house with 1.9-μm C18AQ particles (Dr. Maisch GmbH HPLC) using an Easy nLC-1000 nano-HPLC (Proxeon). Peptides were separated using a linear gradient of 5–30% buffer B over 100 min at 250 nl/min (buffer A = 0.5% (v/v) acetic acid; buffer B = 80% (v/v) acetonitrile, 0.5% (v/v) acetic acid).

Mass analyses were performed using an LTQ Orbitrap Velos Pro or a Q-Exactive plus mass spectrometer (Thermo Scientific). Following each full scan MS1 at 60,000 resolution at 200 m/z (300–1700 m/z; 1×10^6 AGC target), up to 20 most abundant precursor ions were selected for MS/MS (>5000 counts; 2 m/z isolation; 10-ms activation time; activation $q = 0.25$; 35.0 normalized collision energy; minimum charge state of +2; dynamic exclusion of 90 s). Peak lists were generated using Proteome Discoverer v1.4 and submitted to the database search program Mascot (Matrix Science). The data were searched with oxidation (M), acrylamide (C), and carbamidomethyl (C) as variable modifications using a precursor-ion and product-ion mass tolerance of ±10 ppm and ±0.6 Da (±0.02 Da for Q-Exactive plus data), respectively. The enzyme specificity was trypsin with up to two missed cleavages and all taxonomies in the Swiss-Prot database (May 2014; 545,388 entries) were searched. A decoy database of reversed sequences was used to estimate the false discovery rates. To be considered for further analysis, identified peptides had to be top ranking and statistically significant ($p < 0.05$) according to the Mascot expect metric.

Calculation of Gel Stain Intensity Scaling Factors—Three independent fluorescence plots of sucrose gradient-fractionated NuDe/NuRD were subjected to peak fitting in GraphPad Prism v6.07 using the "sum of two Lorentzian curves" function with default options. The resulting best fit values were then used to calculate the proportion of NuRD (*versus* NuDe) in each sucrose gradient fraction. Next, the band intensity was measured by densitometry for each subunit in a SYPRO-Ruby-stained SDS-PAGE of each sucrose gradient fraction. Stoichiometry data for NuRD subunits from previous reports (31, 32) were then averaged (giving RBBP:MTA:GATAD2:HDAC:MBD:CHD ratios of 4.4:2.1:1.6:1:1:0.75) and combined with the densitometry data using the following formula to calculate gel intensity scaling factors for the various NuRD components relative to HDAC1/2.

$$SF = \left(\frac{(\text{gel intensity}) \times (\text{stoichiometry})}{\text{intensity of HDAC1/2}}\right) \quad \text{(Eq. 1)}$$

The scaling factor for CHD4 was further modified to account for the estimated NuRD/NuDe ratio, as calculated above, for each sucrose gradient fraction.

$$SF\,(CHD4) = \left(\frac{(\text{gel intensity}) \times (\text{stoichiometry}) \times (\text{NuRD proportion})}{\text{intensity of HDAC1/2}}\right) \quad \text{(Eq. 2)}$$

Six sucrose gradient fraction samples were used for this calculation. The scaling factor calculated for CHD4 using this method was then used to assess the relative loading of CHD4 in complexes created by supplementing NuDe preparations with recombinant FLAG-CHD4.

Expression and Purification of FLAG-CHD4 in HEK293 Cells—HEK293FT cells were cultured in a humidified atmosphere containing at 37 °C, 5% CO_2 in DMEM, supplemented with 10% (v/v) FBS, 2 mM L-glutamine, 1× minimum essential media nonessential amino acids, 1 mM sodium pyruvate, 50 units/ml penicillin, and 50 μg/ml streptomycin. pcDNA3.1 plasmids encoding for FLAG-CHD4 were transfected into HEK293FT cells at ~70% confluence, and CHD4 protein was expressed for 48–72 h at 37 °C, 5% CO_2. Cells were harvested and resuspended in lysis buffer (50 mM HEPES, 1.5 mM $MgCl_2$, 10 mM KCl, 1 mM DTT, 1 mM PMSF, and 1× cOmplete® protease inhibitor (Roche), pH 7.5). The cells were incubated on ice for 30 min, vortexed, and spun down for 5 min at 3,300 × *g*. The supernatant, consisting of the cytoplasmic fraction, was aspirated and discarded. The nuclear pellet was resuspended in FLAG binding buffer (50 mM HEPES, 0.5 M NaCl, 1 mM EDTA, 1% Triton X-100, 1.5 mM $MgCl_2$, 1 mM DTT, 1 mM PMSF, and 1× cOmplete® protease inhibitor (Roche), pH 8). The nuclear pellet was then homogenized via sonication, incubated on ice for 30 min to allow the chromatin to precipitate, and cleared by centrifugation for 20 min at 16,000 × *g* at 4 °C. The resulting nuclear extract was then incubated with α-FLAG M2 affinity gel beads (Sigma-Aldrich) overnight on a rocker at 4 °C. The next day, the α-FLAG M2 beads were washed with FLAG wash buffer (20 t; 50 mM HEPES, 500 mM NaCl, 0.5% (v/v) IGEPAL® CA-630, 1 mM DTT, pH 7.5), and the FLAG-CHD4 protein was eluted with 300 μg/ml 3×FLAG peptide (MDYKDHDGDYKDHDIDYKDDDDK, in 20 mM HEPES, 150 mM NaCl, 1 mM DTT, and 10% (v/v) glycerol, pH 7.5; ApexBio). Protein samples were analyzed by SDS-PAGE and visualized using SYPRO-Ruby (Life Technologies) and Coomassie stains. All cell culture materials were purchased from Gibco™.

FOG1 Affinity Pulldown with Supplemented CHD4—This purification method was similar to the one described above for FOG1 affinity pulldown with the exception that either purified FLAG-CHD4 was added to NuRD/NuDe prebound to FOG1 peptide immobilized on beads (2 h at 4 °C) or HEK293FT nuclear extract containing expressed FLAG-CHD4 was added the MEL cell nuclear extract prior to incubation with the FOG1 peptide.

Nucleosome Reconstitutions—Nucleosomes were assembled on DNA fragments derived from the 601 nucleosome positioning sequence (54) and purified recombinant *Xenopus laevis* histone octamers, to give a typical final nucleosome concentration of 1–2 μM. Assembly was performed by salt gradient dialysis using a double dialysis method (54), as follows. Reactions were placed in microdialysis buttons, which were placed inside a

dialysis bag containing 30 ml of 1× TE and 2 M NaCl; the dialysis bag was then dialyzed overnight against 2 liters of 1× TE at room temperature and then against a further 1 L of 1× TE for 3–6 h. The histone octamers used in these reactions were assembled using standard protocols from purified recombinant histones (55), either all as unlabeled proteins or containing Alexa Fluor 488-labeled H2A.

Labeling of H2A was achieved via the incorporation of a single cysteine residue at position 120. A synthetic gene encoding H2A-T120C was purchased from GeneArt® and cloned into a rhamnose-inducible pRham vector (Lucigen). H2AT120C was expressed at 37 °C overnight in Rosetta™ 2 (DE3) pLysS *E. coli* cells in ZYP-5052 autoinduction medium (56) containing an additional 0.2% (w/v) rhamnose and then purified from inclusion bodies using standard protocols (55). Labeling of purified H2A-T120C was performed under denaturing conditions in 20 mM Tris, pH 7.0, 7 M guanidine HCl, 5 mM EDTA, and 5 mM TCEP with a ~5-fold molar excess of Alexa Fluor 488 C5 maleimide overnight at 4 °C. The reactions were quenched via the addition of 30 mM β-mercaptoethanol and then purified via gel filtration on a Superdex 200 10/300 column in 20 mM Tris, pH 7.0, 7 M guanidine HCl, 0.1% β-mercaptoethanol. Purified labeled H2A was dialyzed against deionized water with 0.05% (v/v) β-mercaptoethanol overnight at 4 °C, aliquoted, and lyophilized for long term storage. Labeling efficiency was ~65–70%.

DNA fragments were produced by PCR using MyTaq DNA polymerase (Bioline) and fluorophore/quencher labeled primers purchased from Sigma-Aldrich or ATDBio. The PCR products were purified via 0.5× TBE 5% polyacrylamide gel electrophoresis and electroelution. The notation *x*W*y* denotes the 147-bp 601 sequence with flanking DNA of *x* and *y* bp on the upstream and downstream side, respectively.

ATP-driven Nucleosome Remodeling Reactions—Nucleosomes were assembled on BHQ1-labeled 0W47 DNA to generate asymmetric end-positioned nucleosomes. All remodeling reactions were performed at 37 °C. Real time quenched FRET remodeling reactions were performed in a FLUOstar OPTIMA plate reader using Corning® black nonbinding surface half-area 96-well plates and 485P and 520P excitation and emission filters, respectively. The reactions contained 50 nM BHQ1–0W47 Alexa Fluor 488-labeled nucleosomes, 50 mM Tris, pH 7.5, 50 mM NaCl, 3 mM $MgCl_2$, and the enzyme concentrations indicated in the figures. Reactions were monitored for 5 min prior to addition of 1 mM ATP to ensure fluorescence changes were ATP-dependent and then monitored for a further 60–70 min, with data points recorded every 30–40 s. Gel-based remodeling reactions were carried out under identical conditions, except the reactions were stopped by placing them on ice and the addition of 0.5 μg salmon sperm DNA and 4% sucrose prior to electrophoresis on 0.5× TBE 5% polyacrylamide gels. Gels were imaged for Alexa Fluor 488 fluorescence on an FLA-9000 laser scanner.

HDAC Activity Assays—To assess the HDAC activity of NuDe, we used fractions from a FOG-based purification that contained a low proportion of CHD4 (a molar ratio of ~0.01–0.02:1 for CHD4 compared with the other subunits, based on the scaling factors calculated above). HDAC activity was measured using an HDAC activity assay kit (Cayman Chemical Company) as per the manufacturer's instructions. Fluorescence was quantified using an Infinite M1000 Pro plate reader (Tecan). The amount of NuDe complex in each assay was adjusted to contain a total of 25 ng of HDAC. The amount of HDAC in each sample was estimated from SYPRO-Ruby-stained SDS-PAGE gels using a known amount of monomeric BSA as a reference (to allow for comparison of HDAC quantities between different gels). As a positive control, 100 ng of manufacturer-supplied HDAC was used. All samples were assayed twice as technical duplicates.

Author Contributions—J. K. K. L. contributed to the experimental design, performed key experiments, analyzed data, and wrote the manuscript; S. R. W. contributed to the experimental design, performed key initial experiments, and analyzed data; A. P. G. S. contributed to the experimental design, contributed to many experiments, and contributed to manuscript writing; H. S. performed key initial experiments and analyzed data; D. P. R. designed, performed, and analyzed the data for all nucleosome remodeling experiments and contributed to manuscript writing; M. T. performed the HDAC assays and analyzed the associated data, contributed to some experiments, and contributed to manuscript writing; M. B. performed key initial experiments; B. L. P. performed some mass spectrometry experiments; N. E. S. conceived and supervised the project, contributed to the experimental design, performed key initial experiments, and analyzed the data; and J. P. M. conceived and supervised the project, contributed to the experimental design, analyzed the data, and wrote the manuscript.

Note Added in Proof—During the processing of this manuscript, a low-resolution negative-stain EM structure of a subcomplex comprising HDAC1, MTA1, and RBBP4 was published, significantly extending our understanding of NuRD complex architecture. Millard, C. J., Varma, N., Saleh, A., Morris, K., Watson, P. J., Bottrill, A. R., Fairall, L., Smith, C. J., and Schwabe, J. W. (2016) The structure of the core NuRD repression complex provides insights into its interaction with chromatin. *eLife* **5**, e13941.

References

1. Mueller-Planitz, F., Klinker, H., and Becker, P. B. (2013) Nucleosome sliding mechanisms: new twists in a looped history. *Nat. Struct. Mol. Biol.* **20,** 1026–1032
2. Gkikopoulos, T., Schofield, P., Singh, V., Pinskaya, M., Mellor, J., Smolle, M., Workman, J. L., Barton, G. J., and Owen-Hughes, T. (2011) A role for Snf2-related nucleosome-spacing enzymes in genome-wide nucleosome organization. *Science* **333,** 1758–1760
3. Clapier, C. R., and Cairns, B. R. (2009) The biology of chromatin remodeling complexes. *Annu. Rev. Biochem.* **78,** 273–304
4. Yadon, A. N., and Tsukiyama, T. (2011) SnapShot: chromatin remodeling: ISWI. *Cell* **144,** 453.e1
5. Le Guezennec, X., Vermeulen, M., Brinkman, A. B., Hoeijmakers, W. A., Cohen, A., Lasonder, E., and Stunnenberg, H. G. (2006) MBD2/NuRD and MBD3/NuRD, two distinct complexes with different biochemical and functional properties. *Mol. Cell Biol.* **26,** 843–851
6. Hendrich, B., and Bird, A. (1998) Identification and characterization of a family of mammalian methyl-CpG binding proteins. *Mol. Cell Biol.* **18,** 6538–6547
7. Yildirim, O., Li, R., Hung, J.-H., Chen, P. B., Dong, X., Ee, L.-S., Weng, Z., Rando, O. J., and Fazzio, T . G. (2011) Mbd3/NURD complex regulates expression of 5-hydroxymethylcytosine marked genes in embryonic stem cells. *Cell* **147,** 1498–1510
8. Günther, K., Rust, M., Leers, J., Boettger, T., Scharfe, M., Jarek, M., Bart-

kuhn, M., and Renkawitz, R. (2013) Differential roles for MBD2 and MBD3 at methylated CpG islands, active promoters and binding to exon sequences. *Nucleic Acids Res.* **41,** 3010–3021
9. Asturias, F. J., Chung, W. H., Kornberg, R. D., and Lorch, Y. (2002) Structural analysis of the RSC chromatin-remodeling complex. *Proc. Natl. Acad. Sci. U.S.A.* **99,** 13477–13480
10. Chaban, Y., Ezeokonkwo, C., Chung, W. H., Zhang, F., Kornberg, R. D., Maier-Davis, B., Lorch, Y., and Asturias, F. J. (2008) Structure of a RSC-nucleosome complex and insights into chromatin remodeling. *Nat. Struct. Mol. Biol.* **15,** 1272–1277
11. Dechassa, M. L., Zhang, B., Horowitz-Scherer, R., Persinger, J., Woodcock, C. L., Peterson, C. L., and Bartholomew, B. (2008) Architecture of the SWI/SNF-nucleosome complex. *Mol. Cell Biol.* **28,** 6010–6021
12. Leschziner, A. E., Lemon, B., Tjian, R., and Nogales, E. (2005) Structural studies of the human PBAF chromatin-remodeling complex. *Structure* **13,** 267–275
13. Leschziner, A. E., Saha, A., Wittmeyer, J., Zhang, Y., Bustamante, C., Cairns, B. R., and Nogales, E. (2007) Conformational flexibility in the chromatin remodeler RSC observed by electron microscopy and the orthogonal tilt reconstruction method. *Proc. Natl. Acad. Sci. U.S.A.* **104,** 4913–4918
14. Nguyen, V. Q., Ranjan, A., Stengel, F., Wei, D., Aebersold, R., Wu, C., and Leschziner, A. E. (2013) Molecular architecture of the ATP-dependent chromatin-remodeling complex SWR1. *Cell* **154,** 1220–1231
15. Racki, L. R., Yang, J. G., Naber, N., Partensky, P. D., Acevedo, A., Purcell, T. J., Cooke, R., Cheng, Y., and Narlikar, G. J. (2009) The chromatin remodeller ACF acts as a dimeric motor to space nucleosomes. *Nature* **462,** 1016–1021
16. Tosi, A., Haas, C., Herzog, F., Gilmozzi, A., Berninghausen, O., Ungewickell, C., Gerhold, C. B., Lakomek, K., Aebersold, R., Beckmann, R., and Hopfner, K. P. (2013) Structure and subunit topology of the INO80 chromatin remodeler and its nucleosome complex. *Cell* **154,** 1207–1219
17. Smith, C. L., Horowitz-Scherer, R., Flanagan, J. F., Woodcock, C. L., and Peterson, C. L. (2003) Structural analysis of the yeast SWI/SNF chromatin remodeling complex. *Nat. Struct. Biol.* **10,** 141–145
18. Denslow, S. A., and Wade, P. A. (2007) The human Mi-2/NuRD complex and gene regulation. *Oncogene* **26,** 5433–5438
19. O'Shaughnessy, A., and Hendrich, B. (2013) CHD4 in the DNA-damage response and cell cycle progression: not so NuRDy now. *Biochem. Soc. Trans.* **41,** 777–782
20. Yoshida, T., Hazan, I., Zhang, J., Ng, S. Y., Naito, T., Snippert, H. J., Heller, E. J., Qi, X., Lawton, L. N., Williams, C. J., and Georgopoulos, K. (2008) The role of the chromatin remodeler Mi-2β in hematopoietic stem cell self-renewal and multilineage differentiation. *Genes Dev.* **22,** 1174–1189
21. Gao, Z., Huang, Z., Olivey, H. E., Gurbuxani, S., Crispino, J. D., and Svensson, E. C. (2010) FOG-1-mediated recruitment of NuRD is required for cell lineage re-enforcement during haematopoiesis. *EMBO J.* **29,** 457–468
22. Li, X., Jia, S., Wang, S., Wang, Y., and Meng, A. (2009) Mta3-NuRD complex is a master regulator for initiation of primitive hematopoiesis in vertebrate embryos. *Blood* **114,** 5464–5472
23. Lai, A. Y., and Wade, P. A. (2011) Cancer biology and NuRD: a multifaceted chromatin remodelling complex. *Nat. Rev. Cancer* **11,** 588–596
24. Pegoraro, G., Kubben, N., Wickert, U., Göhler, H., Hoffmann, K., and Misteli, T. (2009) Ageing-related chromatin defects through loss of the NURD complex. *Nature Cell Biol.* **11,** 1261–1267
25. dos Santos, R. L., Tosti, L., Radzisheuskaya, A., Caballero, I. M., Kaji, K., Hendrich, B., and Silva, J. C. (2014) MBD3/NuRD facilitates induction of pluripotency in a context-dependent manner. *Cell Stem Cell* **15,** 102–110
26. Luo, M., Ling, T., Xie, W., Sun, H., Zhou, Y., Zhu, Q., Shen, M., Zong, L., Lyu, G., Zhao, Y., Ye, T., Gu, J., Tao, W., Lu, Z., and Grummt, I. (2013) NuRD blocks reprogramming of mouse somatic cells into pluripotent stem cells. *Stem Cells* **31,** 1278–1286
27. Rais, Y., Zviran, A., Geula, S., Gafni, O., Chomsky, E., Viukov, S., Mansour, A. A., Caspi, I., Krupalnik, V., Zerbib, M., Maza, I., Mor, N., Baran, D., Weinberger, L., Jaitin, D. A., *et al.* (2013) Deterministic direct reprogramming of somatic cells to pluripotency. *Nature* **502,** 65–70
28. Millard, C. J., Watson, P. J., Celardo, I., Gordiyenko, Y., Cowley, S. M., Robinson, C. V., Fairall, L., and Schwabe, J. W. (2013) Class I HDACs share a common mechanism of regulation by inositol phosphates. *Mol. Cell* **51,** 57–67
29. Gnanapragasam, M. N., Scarsdale, J. N., Amaya, M. L., Webb, H. D., Desai, M. A., Walavalkar, N. M., Wang, S. Z., Zu Zhu, S., Ginder, G. D., and Williams, D. C., Jr. (2011) p66α-MBD2 coiled-coil interaction and recruitment of Mi-2 are critical for globin gene silencing by the MBD2-NuRD complex. *Proc. Natl. Acad. Sci. U.S.A.* **108,** 7487–7492
30. Alqarni, S. S., Murthy, A., Zhang, W., Przewloka, M. R., Silva, A. P., Watson, A. A., Lejon, S., Pei, X. Y., Smits, A. H., Kloet, S. L., Wang, H., Shepherd, N. E., Stokes, P. H., Blobel, G. A., Vermeulen, M., *et al.* (2014) Insight into the architecture of the NuRD complex: structure of the RbAp48-MTA1 subcomplex. *J. Biol. Chem.* **289,** 21844–21855
31. Kloet, S. L., Baymaz, H. I., Makowski, M., Groenewold, V., Jansen, P. W., Berendsen, M., Niazi, H., Kops, G. J., and Vermeulen, M. (2015) Towards elucidating the stability, dynamics and architecture of the nucleosome remodeling and deacetylase complex by using quantitative interaction proteomics. *FEBS J.* **282,** 1774–1785
32. Smits, A. H., Jansen, P. W., Poser, I., Hyman, A. A., and Vermeulen, M. (2013) Stoichiometry of chromatin-associated protein complexes revealed by label-free quantitative mass spectrometry-based proteomics. *Nucleic Acids Res.* **41,** e28
33. Sims, J. K., and Wade, P. A. (2011) SnapShot: chromatin remodeling: CHD. *Cell* **144,** 626.e1
34. Torchy, M. P., Hamiche, A., and Klaholz, B. P. (2015) Structure and function insights into the NuRD chromatin remodeling complex. *Cell Mol. Life Sci.* **72,** 2491–2507
35. Sun, Y. E., Cheng, L., and Hu, K. (2014) With NuRD, HDACs Go "Nerdy." *Dev. Cell* **30,** 9–10
36. Hong, W., Nakazawa, M., Chen, Y. Y., Kori, R., Vakoc, C. R., Rakowski, C., and Blobel, G. A. (2005) FOG-1 recruits the NuRD repressor complex to mediate transcriptional repression by GATA-1. *EMBO J.* **24,** 2367–2378
37. Lejon, S., Thong, S. Y., Murthy, A., AlQarni, S., Murzina, N. V., Blobel, G. A., Laue, E. D., and Mackay, J. P. (2011) Insights into association of the NuRD complex with FOG-1 from the crystal structure of an RbAp48.FOG-1 complex. *J. Biol. Chem.* **286,** 1196–1203
38. Saathoff, H., Brofelth, M., Trinh, A., Parker, B. L., Ryan, D. P., Low, J. K., Webb, S. R., Silva, A. P., Mackay, J. P., and Shepherd, N. E. (2015) A peptide affinity reagent for isolating an intact and catalytically active multi-protein complex from mammalian cells. *Bioorg. Med. Chem.* **23,** 960–965
39. Mellacheruvu, D., Wright, Z., Couzens, A. L., Lambert, J.-P., St-Denis, N. A., Li, T., Miteva, Y. V., Hauri, S., Sardiu, M. E., Low, T. Y., Halim, V. A., Bagshaw, R. D., Hubner, N. C., al-Hakim, A., Bouchard, A., *et al.* (2013) The CRAPome: a contaminant repository for affinity purification-mass spectrometry data. *Nat. Methods* **10,** 730–736
40. Yang, J. G., Madrid, T. S., Sevastopoulos, E., and Narlikar, G. J. (2006) The chromatin-remodeling enzyme ACF is an ATP-dependent DNA length sensor that regulates nucleosome spacing. *Nat. Struct. Mol. Biol.* **13,** 1078–1083
41. Silva, A. P., Ryan, D. P., Galanty, Y., Low, J. K., Vandevenne, M., Jackson, S. P., and Mackay, J. P. (2016) The N-terminal region of chromodomain helicase DNA-binding protein 4 (CHD4) is essential for activity and contains a high mobility group (HMG) box-like-domain that can bind poly-(ADP-ribose). *J. Biol. Chem.* **291,** 924–938
42. Alkhatib, S. G., and Landry, J. W. (2011) The nucleosome remodeling factor. *FEBS Lett.* **585,** 3197–3207
43. Brownlee, P. M., Chambers, A. L., Oliver, A. W., and Downs, J. A. (2012) Cancer and the bromodomains of BAF180. *Biochem. Soc. Trans.* **40,** 364–369
44. Thompson, P. M., Gotoh, T., Kok, M., White, P. S., and Brodeur, G. M. (2003) CHD5, a new member of the chromodomain gene family, is preferentially expressed in the nervous system. *Oncogene* **22,** 1002–1011
45. Desai, M. A., Webb, H. D., Sinanan, L. M., Scarsdale, J. N., Walavalkar, N. M., Ginder, G. D., and Williams, D. C. (2015) An intrinsically disordered region of methyl-CpG binding domain protein 2 (MBD2) recruits the histone deacetylase core of the NuRD complex. *Nucleic Acids Res.* **43,** 3100–3113
46. Spruijt, C. G., Bartels, S. J., Brinkman, A. B., Tjeertes, J. V., Poser, I.,

Stunnenberg, H. G., and Vermeulen, M. (2010) CDK2AP1/DOC-1 is a bona fide subunit of the Mi-2/NuRD complex. *Mol. Biosyst.* **6,** 1700–1706
47. Wang, Y., Zhang, H., Chen, Y., Sun, Y., Yang, F., Yu, W., Liang, J., Sun, L., Yang, X., Shi, L., Li, R., Li, Y., Zhang, Y., Li, Q., Yi, X., and Shang, Y. (2009) LSD1 is a subunit of the NuRD complex and targets the metastasis programs in breast cancer. *Cell* **138,** 660–672
48. Oates, M. E., Romero, P., Ishida, T., Ghalwash, M., Mizianty, M. J., Xue, B., Dosztányi, Z., Uversky, V. N., Obradovic, Z., Kurgan, L., Dunker, A. K., and Gough, J. (2013) D2P2: database of disordered protein predictions. *Nucleic Acids Res.* **41,** D508–D516
49. Mohan, A., Oldfield, C. J., Radivojac, P., Vacic, V., Cortese, M. S., Dunker, A. K., and Uversky, V. N. (2006) Analysis of molecular recognition features (MoRFs). *J. Mol. Biol.* **362,** 1043–1059
50. Murzina, N. V., Pei, X. Y., Zhang, W., Sparkes, M., Vicente-Garcia, J., Pratap, J. V., McLaughlin, S. H., Ben-Shahar, T. R., Verreault, A., Luisi, B. F., and Laue, E. D. (2008) Structural basis for the recognition of histone H4 by the histone-chaperone RbAp46. *Structure* **16,** 1077–1085
51. Armache, K. J., Garlick, J. D., Canzio, D., Narlikar, G. J., and Kingston, R. E. (2011) Structural basis of silencing: Sir3 BAH domain in complex with a nucleosome at 3.0 A resolution. *Science* **334,** 977–982
52. Sparmann, A., Xie, Y., Verhoeven, E., Vermeulen, M., Lancini, C., Gargiulo, G., Hulsman, D., Mann, M., Knoblich, J. A., and van Lohuizen, M. (2013) The chromodomain helicase Chd4 is required for Polycomb-mediated inhibition of astroglial differentiation. *EMBO J.* **32,** 1598–1612
53. Lazarev, A. V., Rejtar, T., Dai, S., and Karger, B. L. (2009) Centrifugal methods and devices for rapid in-gel digestion of proteins. *Electrophoresis* **30,** 966–973
54. Thåström, A., Lowary, P. T., Widlund, H. R., Cao, H., Kubista, M., and Widom, J. (1999) Sequence motifs and free energies of selected natural and non-natural nucleosome positioning DNA sequences1. *J. Mol. Biol.* **288,** 213–229
55. Luger, K., Rechsteiner, T. J., and Richmond, T. J. (1999) Preparation of nucleosome core particle from recombinant histones. *Methods Enzymol.* **304,** 3–19
56. Studier, F. W. (2005) Protein production by auto-induction in high-density shaking cultures. *Protein Expr. Purif.* **41,** 207–234

CHD4 Is a Peripheral Component of the Nucleosome Remodeling and Deacetylase Complex

Jason K. K. Low, Sarah R. Webb, Ana P. G. Silva, Hinnerk Saathoff, Daniel P. Ryan, Mario Torrado, Mattias Brofelth, Benjamin L. Parker, Nicholas E. Shepherd and Joel P. Mackay

J. Biol. Chem. 2016, 291:15853-15866.
doi: 10.1074/jbc.M115.707018 originally published online May 27, 2016